AD-A159 761 DETERMINATION OF THE SURFACE PHONON DISPERSION 1/1
RELATIONS FOR MONOLAYER BI..(U) CHICAGO UNIV IL JAMES
FRANCK INST K D GIBSON ET AL. AUG 85 TR-8
UNCLASSIFIED N00014-77-C-0240 F/G 20/12 NL

END
FILMED
DTIC

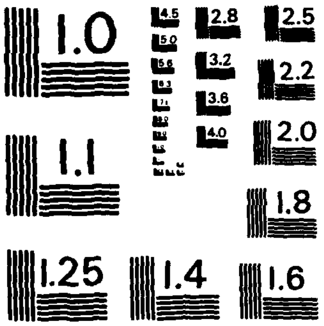

MICROCOPY RESOLUTION TEST CHART
NATIONAL BUREAU OF STANDARDS-1963-A

unclassified

SECURITY CLASSIFICATION OF THIS PAGE (When Data Entered)

(2)

AD-A159 761

REPORT DOCUMENTATION PAGE

READ INSTRUCTIONS BEFORE COMPLETING FORM

1. REPORT NUMBER
8

2. GOVT ACCESSION NO.

3. RECIPIENT'S CATALOG NUMBER

4. TITLE (and Subtitle)
DETERMINATION OF THE SURFACE PHONON DISPERSION RELATIONS FOR MONOLAYER, BILAYER, TRILAYER AND THICK Kr(111) FILMS PHYSISORBED ON Ag(111) BY INELASTIC He SCATTERING

5. TYPE OF REPORT & PERIOD COVERED
Interim Technical Report

6. PERFORMING ORG. REPORT NUMBER

7. AUTHOR(s)
K. D. Gibson and S. J. Sibener

8. CONTRACT OR GRANT NUMBER(s)
N00014-77-C-0240

9. PERFORMING ORGANIZATION NAME AND ADDRESS
The University of Chicago/The James Franck Institute
5640 South Ellis Avenue
Chicago, IL 60637

10. PROGRAM ELEMENT, PROJECT, TASK AREA & WORK UNIT NUMBERS
NR-392-023

11. CONTROLLING OFFICE NAME AND ADDRESS
Office of Naval Research
Physical Sciences Division (Code 421)
800 North Quincy Str., Arlington, VA 22217

12. REPORT DATE
August, 1985

13. NUMBER OF PAGES
15

14. MONITORING AGENCY NAME & ADDRESS(if different from Controlling Office)

15. SECURITY CLASS. (of this report)
unclassified

15a. DECLASSIFICATION/DOWNGRADING SCHEDULE

16. DISTRIBUTION STATEMENT (of this Report)
This document has been approved for public release and sale; its distribution is unlimited.

DTIC
ELECTE
OCT 2 1985
D
B

17. DISTRIBUTION STATEMENT (of the abstract entered in Block 20, if different from Report)

18. SUPPLEMENTARY NOTES
Prepared for publication in Physical Review Letters

19. KEY WORDS (Continue on reverse side if necessary and identify by block number)
Surface phonon spectroscopy; thin film dynamics; phonon dispersion relations; physisorption interactions; gas-surface energy exchange; inelastic single phonon scattering; rare gas interaction potentials

20. ABSTRACT (Continue on reverse side if necessary and identify by block number)

Angle and velocity resolved inelastic He scattering has been used to study how the surface dynamics of thin rare gas films evolve on a layer-by-layer basis. Surface phonon dispersion relations for ordered 1, 2, 3 and 25 layer Kr films physisorbed on Ag(111) are presented along $\bar{\Gamma}\bar{M}$ across the entire Brillouin zone. The monolayer data are dispersionless, indicative of an Einstein oscillator mode. In comparison, the 25 layer film has a well developed Rayleigh wave, typical of a thick crystal surface. Excitation linewidths for monolayer Kr, which vary across the zone, are also briefly discussed. Ori[illegible] Supplied K[illegible] include:

DD FORM 1 JAN 73 1473 EDITION OF 1 NOV 65 IS OBSOLETE

S/N 0102-LF-014-6601

unclassified

SECURITY CLASSIFICATION OF THIS PAGE (When Data Entered)

DTIC FILE COPY

85 10 02 018

A COMPLETE COPY OF THE MANUSCRIPT WILL BE SENT UPON REQUEST.

DETERMINATION OF THE SURFACE PHONON DISPERSION RELATIONS FOR MONOLAYER, BILAYER, TRILAYER AND THICK Kr(111) FILMS PHYSISORBED ON Ag(111) BY INELASTIC He SCATTERING

K. D. Gibson and S. J. Sibener(a)

Department of Chemistry and
The James Franck Institute
The University of Chicago
5640 South Ellis Avenue
Chicago, Illinois 60637

Submitted to Physical Review Letters

(a)Alfred P. Sloan Fellow

PACS: 79.20.Rf; 63.20.Dj; 68.30.+z, 68.60.+q

ABSTRACT

Angle and velocity resolved inelastic He scattering has been used to study how the surface dynamics of thin rare gas films evolve on a layer-by-layer basis. Surface phonon dispersion relations for ordered 1, 2, 3 and 25 layer Kr films physisorbed on Ag(111) are presented along $\bar{\Gamma}\bar{M}$ across the entire Brillouin zone. The monolayer data are dispersionless, indicative of an Einstein oscillator mode. In comparison, the 25 layer film has a well developed Rayleigh wave, typical of a thick crystal surface. Excitation linewidths for monolayer Kr, which vary across the zone, are also briefly discussed.

The physical and chemical properties of atomically thin adsorbed films are currently being examined in great detail by a variety of experimental and theoretical techniques. In addition to their technological importance, studies on these systems are motivated by a desire to understand the many factors, including the essential role played by the underlying substrate, which contribute to the fascinating phenomena associated with them, e.g. a wide diversity of ordered 2-dimensional structures, phase transitions, and novel catalytic activity. To date, much experimental effort has been directed towards elucidating the geometric and electronic properties, i.e., the *static* properties, of these systems. Only recently have vibrational probes, such as low energy electron energy loss spectroscopy [1], inelastic neutron scattering [2], and inelastic He scattering [3] allowed researchers to directly examine the *dynamical* properties of atomically thin films. Of these techniques, inelastic He scattering is the best suited for examining low energy ($\lesssim$ 5 meV) collective excitations since it has excellent energy resolution ($\lesssim$ 250μeV), high surface specificity, and momentum sufficient for probing excitations across the entire surface Brillouin zone (SBZ).

In this Letter we present inelastic He scattering data which demonstrate how the surface phonon dispersion relations for Kr(111) films physisorbed on Ag(111) evolve on a layer-by-layer basis, from monolayer through thick film, across the entire SBZ. These model systems lend themselves to accurate theoretical analysis as a great deal of information exists pertaining to rare gas interaction potentials and rare gas-metal physisorption potentials, including two-body and higher order terms.

The dispersion curves were mapped out using angle resolved He time-of-flight (TOF). The measurements were performed in a UHV scattering apparatus (base pressure $\sim 2 \times 10^{-10}$ torr) equipped with a rotatable and differentially pumped quadrupole mass spectrometer (crystal-to-ionizer distance 14.45 cm, angular resolution 0.67^0). An important feature of the apparatus is that the incident and final polar scattering angles are independently adjustable. Data can therefore be collected across the entire SBZ using a *fixed* incident angle for a given surface; in large part eliminating the necessity of correcting the inelastic transition probabilities for intensity variations that occur due to selective adsorption resonances in the incident channel. The mechanically modulated 18 meV He beam ($\Delta v/v \sim 1\%$, shutter function $\sim 3\mu$sec FWHM) was produced in a liquid nitrogen cooled nozzle beam source. The Ag single crystal was cut and polished to within 0.5^0 of the (111) plane, as confirmed by Laue X-ray back-reflection. Surface cleanliness was checked using Auger spectroscopy. When needed, the crystal was cleaned using Ar^+ bombardment, and subsequently annealed at 750 K. Surface coherence was checked by monitoring the specular scattering lineshape of a 64 meV He beam, and analyzed using simple perturbation theory [4], indicating a coherence length of ca. 100 Å. The azimuthal orientation was determined using H_2 diffraction.

Our thin film growth procedures were guided by extensive information that was already available about the structure and thermodynamics of rare gas overlayers on Ag(111) [5]. Ar, Kr, and Xe form azimuthally aligned but translationally incommensurate lattices on this surface. Monolayers were grown by controlling the pressure of a differentially pumped dosing beam and the surface temperature. Overlayers were grown by subsequent computer controlled deposition on well annealed monolayers. The quality and structure of the Kr surfaces were checked using He diffraction, as shown in Figure 1 for four different overlayers. Specular peak widths and intensities indicate that the coherence lengths of these surfaces are only slightly less than the Ag substrate, i.e, we are not growing roughened films. The very low diffuse scattering seen in Figure 1 also confirms the high quality of the

Kr overlayers. The lattice constant for Kr monolayer, 4.02 Å, is just slightly larger than that for the 2, 3, and 25 layer films, 4.00 Å. When the experiments with an overlayer were completed, the coverage was confirmed using temperature programmed thermal desorption (TPD): a Kr trilayer TPD spectrum is shown in the inset of Figure 3. Since the monolayer desorption peak occurs at a higher temperature than the multilayer peaks, the ratio of the total integrated area to that of the monolayer gives a quantitative measure of the coverage. Only data collected on films typically falling within 5% of a particular overlayer thickness were used in our analysis for 1, 2, and 3 layer structures.

TOF spectra were taken using a multichannel scaler (1μsec/chan dwell time), and required approximately 1 hour of signal averaging. The first step in the analysis was to fit the TOF data using a non-linear least squares routine. Flight times, referenced to the elastic specular TOF, were then used to determine the phonon energies. The parallel momentum exchange of a given peak could then be calculated using the kinematic constraints imposed by the incident and final scattering angles, the phonon energy, and the conservation of crystal momentum. A more detailed description of the experimental apparatus and procedures will be given elsewhere [6].

Figure 2 shows typical TOF spectra for the four different Kr overlayers. The well defined peaks indicate that single phonon exchanges are the dominant inelastic scattering channel. Each TOF spectrum also includes an elastic feature, which we attribute to incoherent scattering from crystal defects. The computer simulations in Fig. 2 are forward convolutions which have been scaled to show excitation lineshapes, but *not* probabilities, and which i) use as input the experimental dispersion curves ii) include the instrument transfer function and iii) assume single phonon exchanges having delta-function energy widths. When the phonon excitation lineshapes are allowed to have *finite* energy widths, the simulations in most cases fit the experimental spectra, yielding information on phonon relaxation [6]. Most of the spectra were intentionally taken at the same incident angle ($\theta_i = 45^0$). An observation made on Xe monolayers indicates why a constant incident angle should be used for quantitatively examining inelastic transition probabilities: it was found that the intensities of the inelastic peaks did not scale linearly with the specular beam at two two slightly different incident angles due to the presence of a selective adsorption resonance in the incident channel. Such resonances are common and pronounced features on all of the rare gas systems we have examined [7]. (Our scattering geometry does not eliminate intensity variations that are due to resonances in the exit channel.)

Figure 3 is a reduced zone plot of the principal modes observed on the 1, 2, 3 and 25 layer layer Kr films. Only the energy loss and gain features adjacent to the elastic TOF in Fig. 2 are plotted. The layer-by-layer evolution of the surface dynamics of these structures is clearly revealed, with striking differences apparent between the monolayer and 25 layer film.

The monolayer $SP_\perp$ mode, the only mode we observe, is dispersionless within our experimental error. This indicates that the physisorbed Kr atoms are behaving as independent Einstein oscillators, vibrating in an uncorrelated manner in the well of the holding potential, V(z). We note that this behavior has also been directly observed [3, 8, 9], and indirectly inferred [10], for rare gases physisorbed on graphite and other metallic surfaces. The monolayer $SP_\perp$ frequency allowed us to determine the second derivative of V(z) at the equilibrium position, and hence the force constant, $k_{Kr-Ag} = 171$ meV-$Å^{-2}$. Using this parameter in conjunction with the previously determined well depth (D = 108 mev) [11], C_3 constant and reference plane ($C_3 = 2263$ meV-$Å^3$, $z_0 = 0.2521$ Å) [12], we have derived an exponential-3 parameterization of the holding potential [6], $V(z) = A\exp(-\beta(z-z_0))-C_3/(z-z_0)^3$, with A = 21556 meV and $\beta = 2.407$ $Å^{-1}$ (this potential is not valid for small z as no saturation term was included to account for the singularity at z_0). This analysis demonstrates that information on physisorption potentials for heavy adsorbates can be obtained using inelastic He scattering, complementing the selective adsorption techniques that are applicable for light adparticles [13]. Fitting the bottom of the well with a Morse potential shows V(z) to be nearly harmonic up to level n = 5. Figure 4 is a plot of all the inelastic peaks for the monolayer. The average energies are, from bottom to top, 2.93, 5.82, and 8.78 meV--corresponding to 1, 2, and 3 times the fundamental within the precision of our measurements. Since the potential is harmonic near its minimum, and the oscillators are at or near the ground state for the surface temperature of these experiments (25 ± 1 K), we can not yet unambiguously determine the relative contribution from multiphonon and overtone excitations. Detailed comparisons between the experimental transition probabilities (including temperature dependent data) and those from scattering calculations, assuming either overtone or multiphonon excitations, should help clarify this situation.

As further overlayers are added there is increasing dispersion (Fig. 3), until at 25 layers a well developed Rayleigh mode is seen. The energy at the $\bar{M}$ point (short wavelength limit) is very nearly the bulk value after adsorbing only two layers. Not surprisingly, the convergence to bulk-like behavior is much slower at $\bar{\Gamma}$, where displacements can extend well below the surface [1]. We were unable to extend the 25 layer measurements to $\underset{\sim}{Q}/\underset{\sim}{Q}_{max} < 0.25$ because the weak inelastic TOF peak merged with the tail of the strong elastic signal. Also note that not all of the points plotted in Figs. 3 and 4 are for normal processes, $\underset{\sim}{G} = (00)$. Inelastic transitions involving Umklapp phonons are in fact quite strong due to the high corrugation of the He-Kr(111) potential. All four possible combinations of $\Delta\underset{\sim}{Q}$ and ΔE are observed.

The dispersion curves were primarily mapped out by tracking the most intense energy loss feature across the first SBZ for $\underset{\sim}{Q} < 0$ (parallel momentum loss with respect to the scattered He). The experimental intensity for this peak was $\sim 10^{-3}$ of the specular beam and $\sim 10^{-4}$ of the incident beam, with a variation of no more than a factor of 5 across the SBZ. This small change in transition probability as a function of $\underset{\sim}{Q}$ differs from the large exponential fall-off found on metals [14], and is partly due to the larger "cut-off factor", Q_c [15], for this system [6,16].

Theoretical dispersion curves for these overlayers have recently been derived [17, 18, 19]. These lattice dynamics results fit the experimental data quite well when realistic rare gas pair potentials and physisorption potentials are used in the calculation. The agreement between theory and experiment gives further evidence that the examined rare gas films order in a layer-by-layer fashion on Ag(111), i.e. exhibit Type 1 growth [20].

We are now examining deconvoluted inelastic transition probabilities and lineshapes. In our preliminary analysis one interesting trend has already been observed which is related to phonon lifetimes: at small $\underset{\sim}{Q}$, when the adsorbate's Einstein mode overlaps the surface vibrational modes of the substrate, the linewidths are on the order of 1 meV FWHM; whereas at large $\underset{\sim}{Q}$, where there is no overlap and the decay pathway is anharmonic, linewidths are relatively narrow, $\lesssim 0.25$ meV. These observations, and the others reported above, convincingly demonstrate that inelastic He scattering can be used to study the surface dynamics of overlayers, complementing elastic diffraction and selective adsorption measurements which yield information on static properties [7, 13].

Acknowledgements

We would like to thank C. F. Yu and D. Padowitz for experimental assistance and B. M. Hall, D. L. Mills, and J. E. Black for their theoretical collaboration. We also thank M. B. Webb, L. W. Bruch, and M. L. Klein for valuable discussions. This work was supported, in part, by the ONR and the NSF-MRL at the University of Chicago. S. J. Sibener also acknowledges support from a Camille and Henry Dreyfus Foundation Young Faculty Grant, and an I.B.M. Faculty Development Award.

References

[1] H. Ibach and D. L. Mills, Electron Energy Loss Spectroscopy and Surface Vibrations (Academic Press, New York, 1982).

[2] J. P. McTague, M. Nielson, and L. Passell, in Chem. and Phys. of Solid Surfaces V.II (CRC Press, R. Vanselow, Ed., 1979).

[3] B. F. Mason and B. R. Williams, Surf. Sci. 111, 609 (1981).

[4] J. M. Ziman, Principles of the Theory of Solids (Cambridge Univ. Press, Cambridge, 1972), p. 56.

[5] J. Unguris, L. W. Bruch, E. R. Moog, and M. B. Webb, Surf. Sci. 87, 415 (1979); J. Unguris, L. W. Bruch, E. R. Moog, and M. B. Webb, Surf. Sci. 109, 522 (1981).

[6] K. D. Gibson and S. J. Sibener, to be published.

[7] K. D. Gibson and S. J. Sibener, to be published.

[8] H. Taub, K. Carneiro, J. K. Kjems, L. Passell, and J. P. McTague, Phys. Rev. B16, 4551 (1977).

[9] B. F. Mason and B. R. Williams, Surf. Sci. 139, 173 (1984).

[10] T. H. Ellis, G. Scoles, and U. Valbusa, Chem. Phys. Lett. 94, 247 (1983).

[11] L. W. Bruch, Surf. Sci. 125, 194 (1983).

[12] E. Zaremba and W. Kohn, Phys. Rev. B13, 2270 (1976).

[13] H. Hoinkes, Rev. Mod. Phys. 52, 933 (1980).

[14] V. Celli, G. Benedek, U. Harten, J. P. Toennies, R. B. Doak, and V. Bortolani, Surf. Sci. 143, L376 (1984).

[15] V. Bortolani, A. Franchini, F. Nizzoli, G. Santoro, G. Benedek and V. Celli, Surf. Sci. 128, 249 (1983).

[16] J. E. Black, private communication.

[17] K. D. Gibson, S. J. Sibener, B. M. Hall, D. L. Mills, and J. E. Black, J. Chem. Phys., to be published.

[18] G. G. Cardini, S. F. O'Shea, M. Marchese, and M. L. Klein, to be published.

[19] L. W. Bruch, private communication.

[20] J. A. Venables, G. D. T. Spiller, and M. Hanbüchen, Rep. Prog. Phys. 47, 399 (1984).

Figure Captions

Figure 1. He diffraction spectra for Kr overlayers physisorbed on Ag(111), taken along the $<11\bar{2}>$ direction, with $\theta_i = 45^0$, $E_i = 18$ meV, and $T_s = 25$ K. The four spectra were collected using the same conditions, so the intensities are directly comparable. Arrows indicate the angles at which the TOF spectra of Fig. 2 were taken.

Figure 2. Typical TOF spectra for Kr overlayers physisorbed on Ag(111), taken with the same parameters as in Fig. 1. Crosses are experimental data, solid lines are least-squares fits, and dashed lines are simulations (see text). Arrows indicate the position of elastic time-of-flight.

Figure 3. Phonon dispersion curves of the Kr overlayers from $\bar{\Gamma} \rightarrow \bar{M}$. Open symbols are for energy loss of the beam, filled-in symbols are for energy gain. Representative error bars are shown for energy and momentum loss features (with respect to the incident beam) which occurred in the first zone, i.e. for normal processes. Solid lines are polynomial fits to the data. The inset is a typical TPD spectrum for a trilayer. Such spectra were essential as their integrated areas were used to confirm the Kr coverage of each film.

Figure 4. Dispersion curves for monolayer Kr/Ag(111), showing the three observed frequencies. Open and filled-in symbols have the same meaning as in Fig. 3.

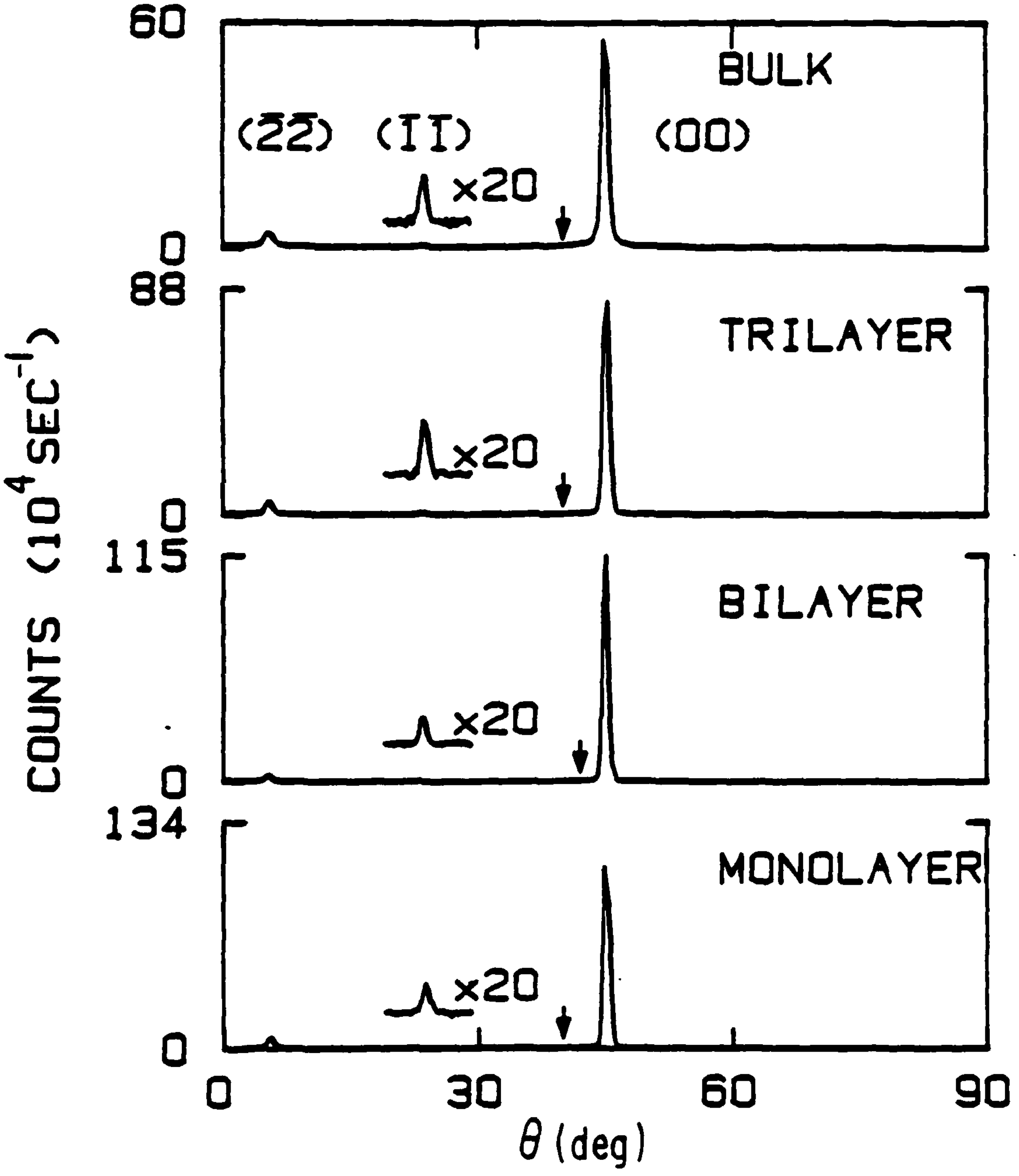
60
BULK
$(\bar{2}\bar{2})$
(11)
(00)
x20
0
88
TRILAYER
x20
0
115
BILAYER
x20
0
134
MONOLAYER
x20
0
0
30
60
90
θ (deg)
COUNTS (10^4 SEC^{-1})

FIGURE 1

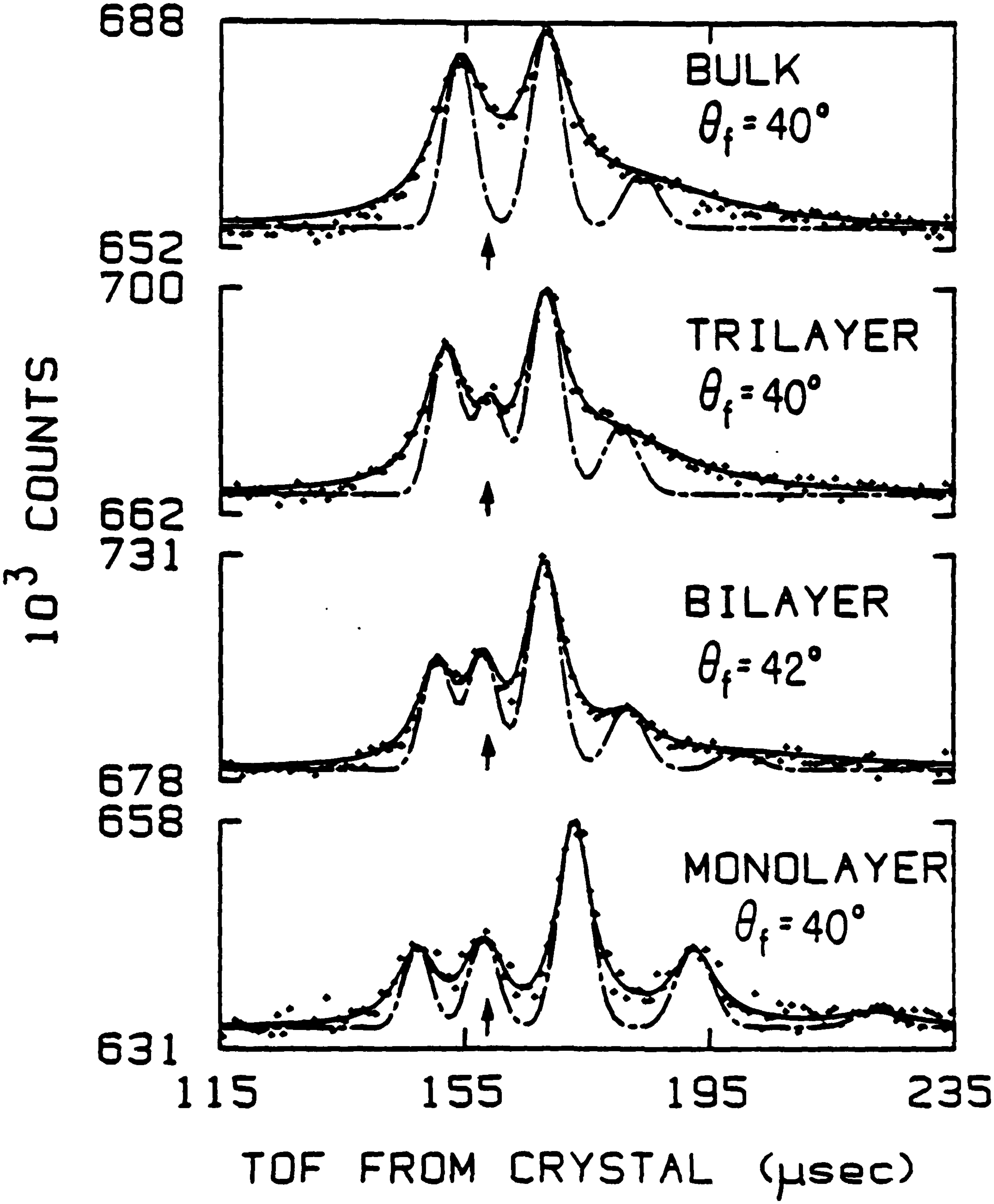
688
652
BULK
$\theta_f = 40°$
700
662
TRILAYER
$\theta_f = 40°$
731
678
BILAYER
$\theta_f = 42°$
658
631
MONOLAYER
$\theta_f = 40°$
10^3 COUNTS
115
155
195
235
TOF FROM CRYSTAL (μsec)

FIGURE 2

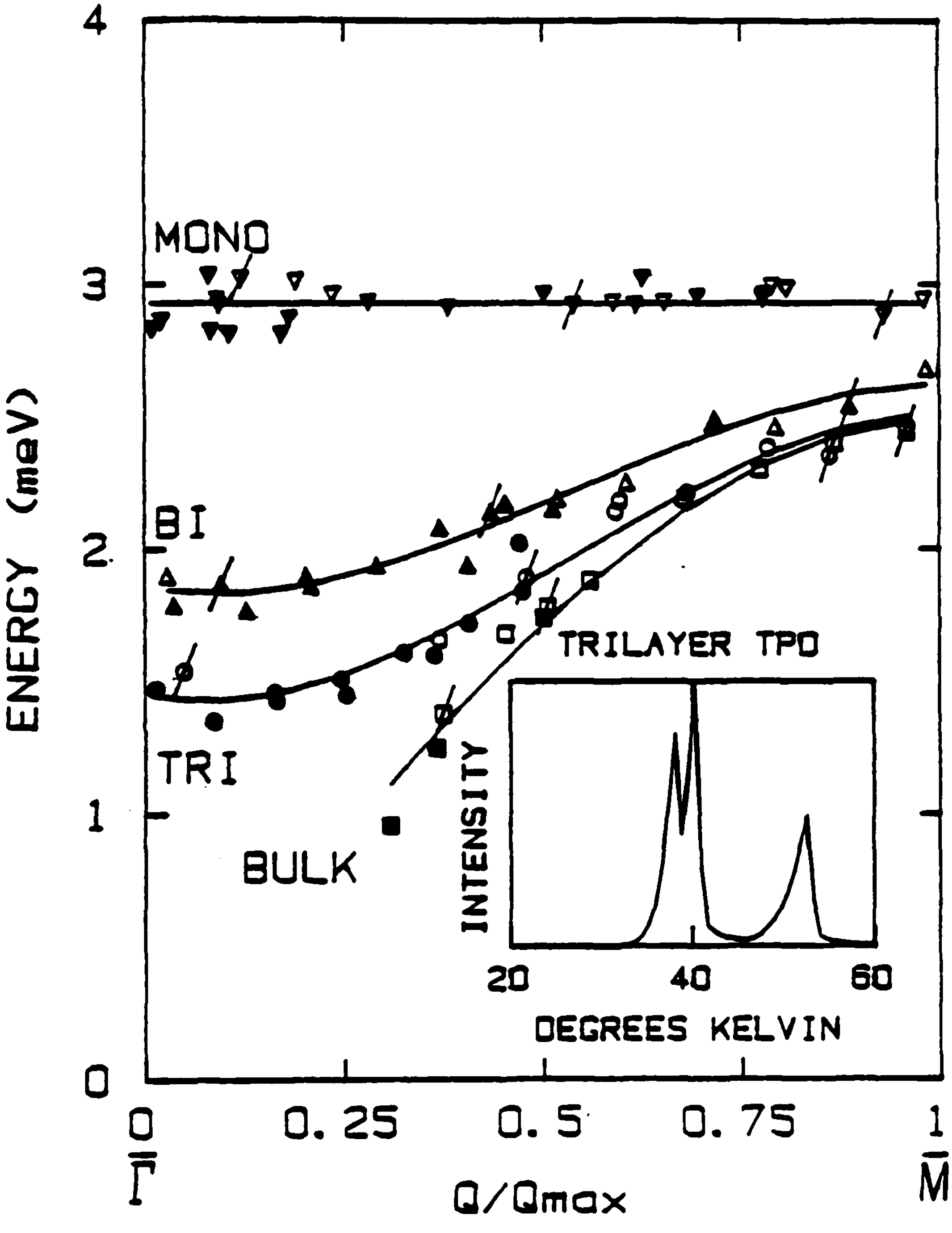
MONO
BI
TRI
BULK
TRILAYER TPD
INTENSITY
20
40
60
DEGREES KELVIN
ENERGY (meV)
0
1
2
3
4
0
0.25
0.5
0.75
1
Γ̄
M̄
Q/Qmax

FIGURE 3

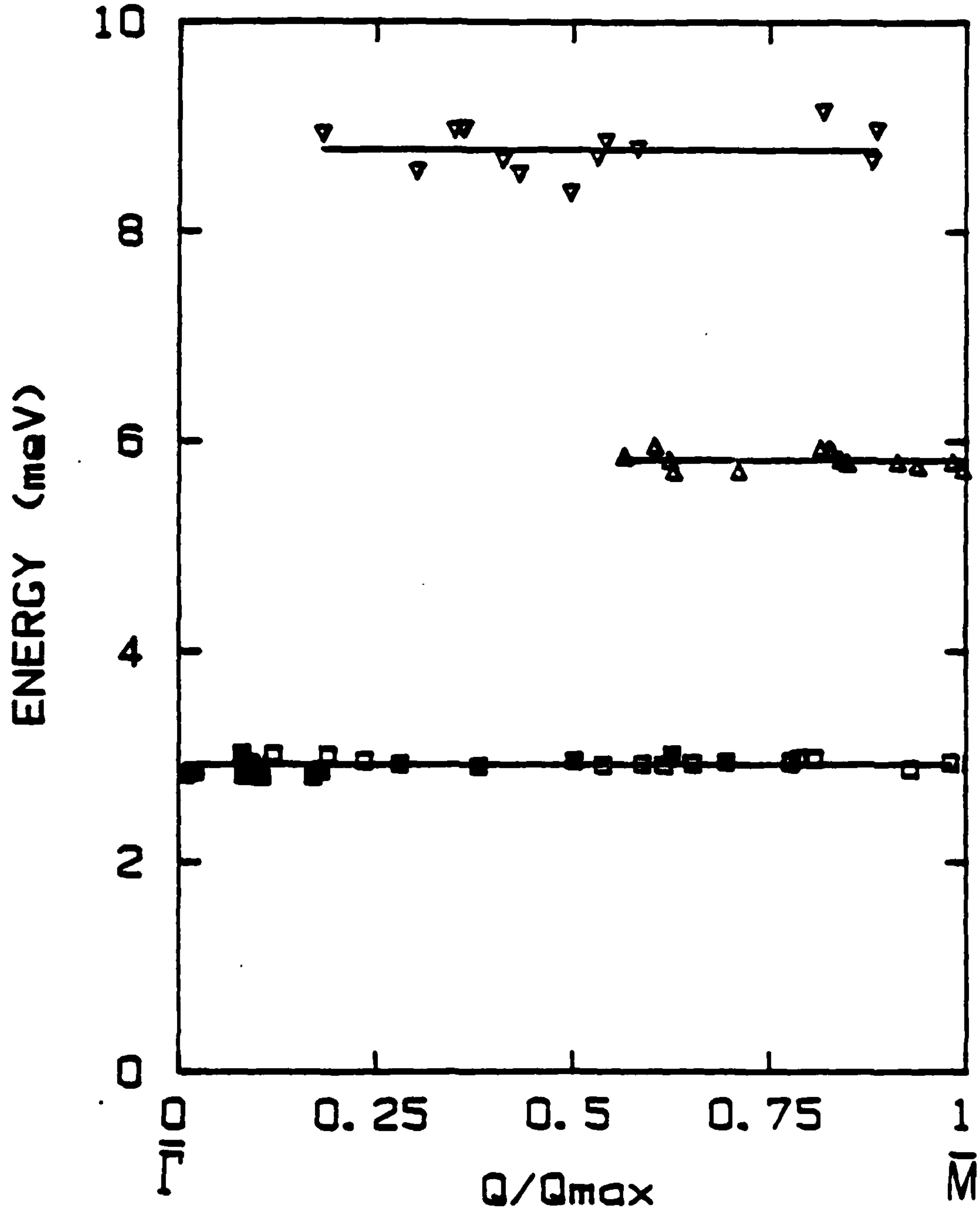

FIGURE 4